Cambridge Centre for Computational Chemical Engineering

University of Cambridge

Department of Chemical Engineering and Biotechnology

Preprint ISSN 1473 – 4273

Modelling the Internal Structure of Nascent Soot Particles

Tim S. Totton[1], Dwaipayan Chakrabarti[3], Alston J. Misquitta[2],

Markus Sander[1], David J. Wales[3], Markus Kraft[1]

released: 17 July 2009

[1] Department of Chemical Engineering and Biotechnology
University of Cambridge
New Museums Site, Pembroke Street
Cambridge CB2 3RA
United Kingdom

[2] Department of Physics
Cavendish Laboratory
University of Cambridge
J J Thomson Avenue
Cambridge, CB3 0HE
United Kingdom

[3] Department of Chemistry
University Chemical Laboratories
University of Cambridge
Lensfield Road
Cambridge, CB2 1EW
United Kingdom

Preprint No. 77

c4e

Key words and phrases: PAH, soot modelling, intermolecular potentials

Edited by
Cambridge Centre for Computational Chemical Engineering
Department of Chemical Engineering and Biotechnology
University of Cambridge
Cambridge CB2 3RA
United Kingdom.

Fax: + 44 (0)1223 334796
E-Mail: c4e@cheng.cam.ac.uk
World Wide Web: http://www.cheng.cam.ac.uk/c4e/

Abstract

In this paper we present studies of clusters assembled from polycyclic aromatic hydrocarbon (PAH) molecules similar in size to small soot particles. The clusters studied were comprised of coronene ($C_{24}H_{12}$) or pyrene ($C_{16}H_{10}$) molecules and represent the types of soot precursor molecule typically found in flame environments. A stochastic 'basin-hopping' global optimisation scheme was used to locate low-lying local minima on the potential energy surface (PES) of the molecular clusters. TEM-style projections of the resulting geometries show similarities with those observed experimentally in TEM images of soot particles. The mass densities of these clusters have also been calculated and are lower than bulk values of the pure crystalline PAH structures. They are also significantly lower than the standard value of 1.8 g/cm^3 used in our soot models. Consequently we have varied the mass density between 1.0 g/cm^3 and 1.8 g/cm^3 to examine the effects of varying soot density on our soot model and observed how the shape of the particle size distribution changes. Based on similarities between nascent soot particles and PAH clusters a more accurate soot density is likely to be significantly lower than 1.8 g/cm^3. As such, for modelling purposes, we recommend that the density of nascent soot should be taken to be the value obtained for our coronene cluster of 1.12 g/cm^3.

Contents

1 Introduction

The mechanisms by which soot precursor molecules, such as polycyclic aromatic hydrocarbon (PAH) molecules, form a soot 'particle' in the gas phase remain poorly understood. Likewise, little is known about the internal structure of soot other than from HRTEM images [1, 2] and the results of some numerical studies of PAH interactions which have investigated clustering and the dynamics of the molecular interactions [3–7]. Developing an understanding of the internal structure of soot particles is essential to improve our current soot models [8–17]. In particular it is vital to establish how molecules arrange locally and how mobile they are within a particle to properly understand the time evolution of soot particles in flame environments. For example, information on internal structure is necessary to understand how steric hindrance within the particle affects reaction rates with gas phase species. Similarly the transport properties of the gas phase species around the particle surface and through the particle will depend on the local molecular arrangement. Understanding the mobility of PAHs within the particle and around the surface will also help determine the degree to which aggregated soot particles can change their morphology. In order to gain such detailed information about internal structure it is necessary to study the potential energy surface (PES) associated with the molecular cluster and currently the only way to do this in a computationally feasible manner is to use model intermolecular potentials.

Intermolecular potentials are used to describe the interactions between molecules in 'weakly bound' systems where a variety of individual interactions determine the overall interaction. The overall interaction energy of a molecular cluster can be approximated as the sum over all pairwise atom-atom interactions:

$$U = \sum_{A} \sum_{A<B} \sum_{a \in A} \sum_{b \in B} U_{ab}(R_{ab}, \Omega_{ab}), \tag{1}$$

where $U_{ab}(R_{ab}, \Omega_{ab})$ denotes an atom-atom or site-site interaction potential. The indices A and B are for molecules, and the indices a and b run over all the atomic interaction sites within a molecule. In general the interaction potential depends upon the atom-atom separation, R_{ab}, which is the separation between atom a in molecule A and atom b in molecule B, and the relative molecular orientation, described in some way by Ω_{ab}. Often, however, orientational dependence is removed as a simplification and such potentials are 'isotropic', *i.e.* they treat each atom in a given molecule as if it has a uniform electron distribution around it.

Two terms that are universal in model potentials are the repulsion and dispersion contributions. Other terms such as electrostatic or polarisation interactions can also be added on an atom pair basis. There have been many different forms suggested for U_{ab}, with perhaps the simplest being the Lennard-Jones (L-J) 6-12 potential:

$$U_{\mathrm{LJ}} = 4\epsilon_{ab}\left[\left(\frac{\sigma_{ab}}{R_{ab}}\right)^{12} - \left(\frac{\sigma_{ab}}{R_{ab}}\right)^{6}\right], \tag{2}$$

where ϵ_{ab} and σ_{ab} are usually empirically derived and correspond to the potential well-depth and size parameters describing the interaction between atoms a and b. The R^{-12}

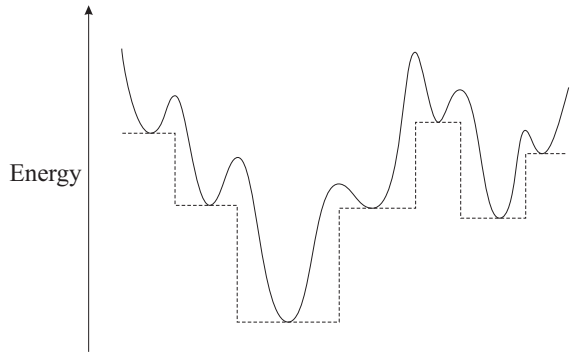

Figure 1: *A schematic diagram illustrating the effects of the basin-hopping energy transformation for a one-dimensional example. The solid line is the energy of the original surface and the dashed line is the transformed energy* $\widetilde{E}$.

term represents repulsion whilst the R^{-6} term represents dispersion. A simple point charge term to model the electrostatic interaction explicitly is often added and takes the following form:

$$U_{\text{elec}} = \left(1389.963 \frac{\text{kJ}}{\text{mol}} \frac{\text{Å}}{\text{e}^2}\right) \frac{q_a q_b}{R_{ab}}, \tag{3}$$

where q_a and q_b represent partial charges located at nuclear positions within molecules A and B respectively.

Using a model potential the potential energy surface (PES) for a molecular cluster can be generated and scanned to find low-lying minima, which correspond to energetically favourable geometries. In the present work a global optimisation scheme based on the 'basin-hopping' method [18] has been used. This approach uses a simple transformation of the energy landscape which does not change the global minimum, or the relative energies of the local minima:

$$\widetilde{E}(\vec{R}) = \min\{E(\vec{R})\}, \tag{4}$$

where 'min' signifies that an energy minimisation is performed, which locates a local minimum on the PES [19]. The transformed energy, $\widetilde{E}(\vec{R})$, for any arrangement of nuclear coordinates, $\vec{R}$, becomes the energy of the structure obtained by minimisation. Each local minimum is, therefore, surrounded by a plateau of constant energy consisting of all the neighbouring geometries from which that particular minimum is obtained (Fig. 1).

The PES is thus transformed into a discrete set of energy levels, which, when combined with a search scheme, can be used to find the associated minima. In the simplest basin-hopping scheme steps are proposed by perturbing the current coordinates and carrying out a minimisation from the resulting geometry. A step is accepted if the energy of the new minimum, E_{new}, is lower than the starting point, E_{old}. If E_{new} is greater than E_{old} then the step is accepted or rejected based on an accept-reject scheme such as the Metropolis criterion. Such a scheme allows the search to escape from traps and survey other regions of the PES.

In this work clusters of PAH molecules have been investigated using a simple 'Lennard-Jones plus point charges' potential [20] with the basin-hopping method. For the first time

we show cluster arrangements of the size of small soot particles. We have calculated the density of these clusters and compared the values with densities found experimentally for bulk coronene and pyrene crystal structures as well as the density of soot. We have also briefly studied the effects of varying soot mass density in our soot models on the particle size distribution to observe how sensitive our models are to this parameter.

2 Results and Discussion

2.1 Molecular Clusters

As PAH molecules are relatively inflexible, it is reasonable to treat the atomic interaction sites within a rigid-body framework, *i.e.* atoms within a molecule are fixed with respect to one another. As such the GMIN basin-hopping code [19, 21] has been used to study clusters of coronene ($C_{24}H_{12}$) and pyrene ($C_{16}H_{10}$) molecules based on the isotropic Lennard-Jones plus point charges atom-atom potential [20]. This code can only study homomolecular clusters in its present form, so studies of mixtures of PAHs were not possible. The Lennard-Jones contribution has been parameterised for simple organic molecules [20] (Table 1), whilst molecular geometries and electrostatic-potential-fitted point charges were taken from the work reported in ref. [6].

Table 1: *Parameters for the Lennard-Jones potential [20]*

Atom Pair	ϵ / kJ/mol	σ / Å
C C	0.3926	3.475
C H	0.1435	3.208
H H	0.0543	2.937

Large homomolecular clusters were considered up to the size of 50 molecules (Figure 2). In the simulations the molecules were initially randomly orientated and scattered whilst ensuring no molecular overlap. The GMIN basin-hopping code was then used to minimise the total potential energy of the cluster by altering the positions and orientations of the constituent molecules. Once a minimum was reached the accept-reject scheme described above was applied allowing the search to jump between basins on the PES by randomly rearranging molecules and minimising again.

For these clusters of many molecules a number of low-lying minima were located, but because of the stochastic nature of the PES search, and the high dimensional nature of the configurational space, it is hard to find the true global minima. However, in the context of flame environments, where soot formation is kinetically controlled and occurs rapidly [22], it is unlikely that configurations would actually locate the global minimum structure. Rather, it is likely that a local minimum is found, which due to further condensation of PAH molecules on the particle surface, becomes trapped on the PES with high energy barriers preventing the inner core of the cluster rearranging to the global minimum structure. Recent experimental studies of soot particles by Vander Wal *et al.* seem to support the notion of an amorphous centre trapped by a crystalline outer shell [1].

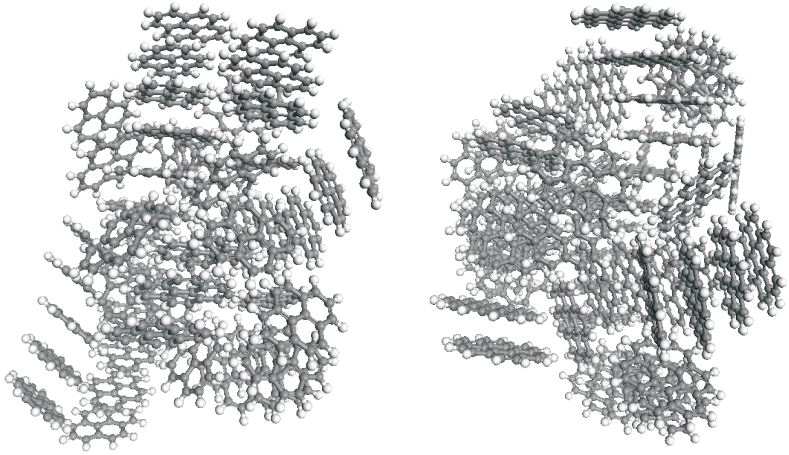

(a) $E/N = -65.8\,kJ/mol$ **(b)** $E/N = -105.5\,kJ/mol$

Figure 2: *Low energy molecular clusters of (a) 50 pyrene molecules and (b) 50 coronene molecules, where E/N is the total interaction energy per molecule.*

The potential energy surface is independent of temperature, but this landscape is sampled at finite temperature in experiments. The stability of the structures we have characterised in flame environments can be roughly estimated by comparing the cluster interaction energies to the average internal energies. The six degrees of freedom from translation and rotation result in an internal energy of $3kT$ per molecule in the cluster [23]. At a typical flame temperature of 1800 K the average internal energy per molecule is 44.9 kJ/mol, which is less than half the absolute value of the interaction energy per molecule for coronene, and approximately two thirds of the equivalent value for pyrene. This result suggests that both clusters may exist for a finite time in such environments but the lifetime of the coronene cluster is expected to be significantly longer than that of the pyrene cluster.

Figure 3(a) shows a projection of a cluster of 50 coronene molecules to indicate how it might appear using transmission electron microscopy and for comparison with the experimental HR-TEM images [Fig. 3(b)]. The average number of molecules found in stacks within the clusters was found to be 3.85 and 2.78 for the coronene and pyrene clusters respectively indicating that larger PAHs will tend to adopt more crystalline arrangements. The separation between molecular planes for both clusters was found to vary between 3.4–3.6 Å, depending on the number of molecules in a given stack, and this compares to a layer separation of 3.5 Å for diesel soot [24] and 3.35 Å for graphite. Whilst the experimental HR-TEM images indicate the presence of PAH structures much larger than coronene, we note that there are similarities in the type of structure seen and the layer separations between stacked PAH molecules.

2.2 Particle Density

To establish the density, ρ, of the molecular clusters a molecular volume must be defined. Our definition uses van der Waals radii [25], treating atoms as solid spheres with a defined

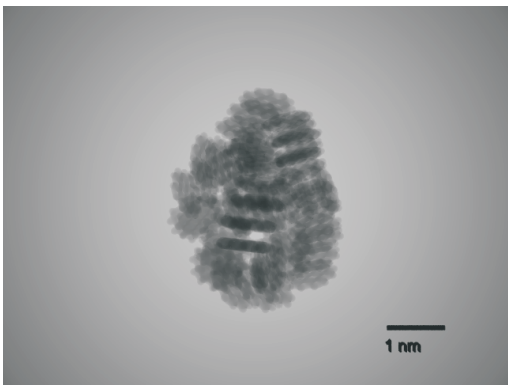

(a) *A TEM-style projection of a cluster of 50 coronene molecules*

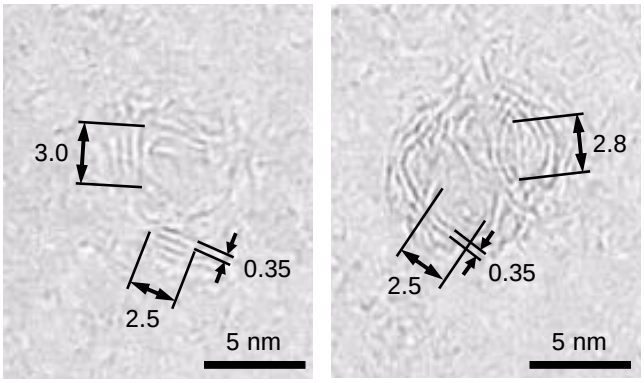

(b) *Experimental HR-TEM images of an aggregate sampled from a diesel engine. Indicated are length scales of structures within a primary particle [24]*

Figure 3: *Comparison of TEM-style projection for a coronene cluster with the experimental HR-TEM of a soot aggregate*

volume, generally obtained from crystallographic data. The radii for hydrogen and carbon were taken from ref. [25] as 1.20 Å and 1.70 Å, respectively. The volume of the cluster, V, can then be altered by a simple scaling factor, α, which scales the predefined van der Waals radii. A Monte Carlo integration scheme [26] was used in which a 'minimum bounding box' that completely enclosed each cluster was calculated and random samples of the box were taken. If the sample points lay within the spheres defined by the scaled radii then they were counted. A million samples were taken and the volume of the cluster was calculated as the ratio of counted points to the total number of samples multiplied by the minimum bounding box volume.

Figure 4(a) shows how the cluster volumes vary non-linearly with scaling factor and it thus becomes necessary to define a critical scaling factor for which a molecular volume, and hence density, are defined. The scaling factor should be chosen such that all intermolecular space within the cluster is encompassed. As the scaling factor increases the volume initially rises as α^3, since no spheres will initially overlap. As spheres begin to overlap, firstly within molecules, and then between molecules, the dependence of V on

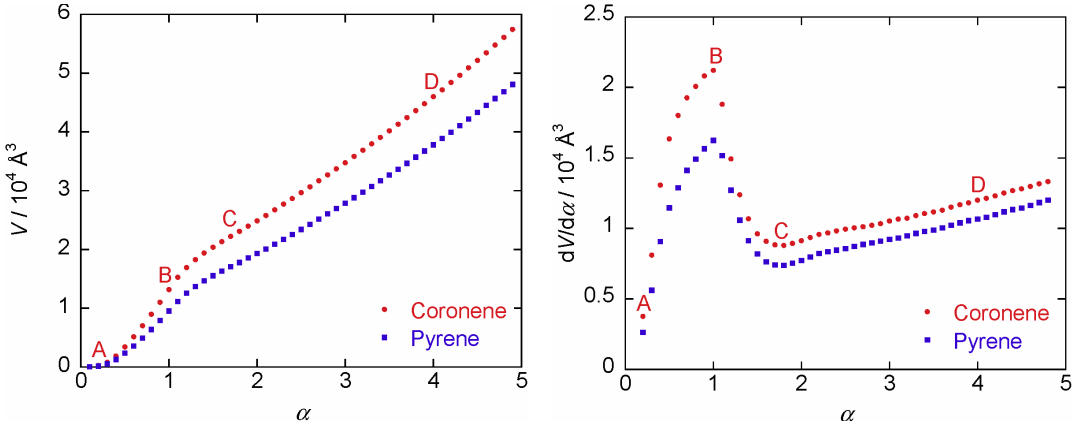

(a) *Volume of coronene$_{50}$ and pyrene$_{50}$ clusters.* **(b)** *First derivative of cluster volume with respect to scaling factor.*

Figure 4: *Defining a critical scaling factor. Letters on the plots correspond to specific scaling factors shown in Fig. 5 for the coronene$_{50}$ cluster.*

α will weaken. When all intermolecular space is encompassed further increase in α will only result in volume growth at the cluster surface. Eventually the volume will return to a cubic dependence as the scaled radii approach the size of the cluster radius. The point of inflexion along this curve was taken as the point at which all intermolecular space was encompassed and hence represented the cluster volume for the critical scaling factor. Plotting the first derivative of the volume against the scaling factor, defined in Eqn. 5, reveals a minimum at $\alpha = 1.7$ for both clusters [Fig. 4(b)].

$$\left.\frac{\mathrm{d}V}{\mathrm{d}\alpha}\right|_n \approx \frac{1}{2}\left(\frac{V_{n+1} - V_n}{\alpha_{n+1} - \alpha_n} + \frac{V_n - V_{n-1}}{\alpha_n - \alpha_{n-1}}\right) \tag{5}$$

Using this scaling factor the densities of the coronene and pyrene clusters are 1.12 g/cm^3 and 0.98 g/cm^3, respectively. These values are approximately 80% of the bulk densities of solid coronene and pyrene, which are 1.38 g/cm^3 and 1.27 g/cm^3 respectively. These bulk values represent crystal structures with high order, so molecular clusters trapped in local minimum configurations, with little long-range order are expected to have lower densities. The change in density observed from pyrene to coronene clusters is largely due to the greater mass of coronone molecules combined with a similar interplanar spacing for the molecular stacks. The coronene molecules also tend to arrange on average into more efficient stacks than the pyrene molecules. It can be expected that homomolecular clusters of larger PAHs would have higher density although the packing efficiency is important as shown by the difference between the bulk crystalline densities and those of the cluster. An ensemble of different PAHs is expected in soot [27, 28], yet despite likely possessing PAHs larger than coronene such clusters will be unlikely to exhibit the same packing efficiency and thus density may not be considerably greater.

Whilst the calculated densities correspond to pure component coronene and pyrene clusters it is clear that they have some implications for the density of nascent soot particles which we consider to be clusters of PAH molecules. Dobbins *et al.* [28] have studied the composition of nascent soot particles in flames and highlight that PAHs with between

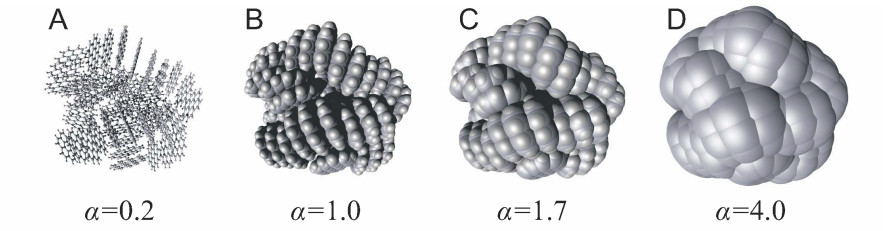

Figure 5: *50 coronene cluster at various scaling factors*

20–24 carbon atoms are most common. A cluster of coronene molecules is therefore not an unreasonable approximation to a nascent soot particle. Our models currently assume a soot mass density of 1.8 g/cm^3 [29, 30], however this is likely to be too large when considering soot particles soon after inception, when structure is more amorphous. We propose a better estimate of the mass density of nascent soot to be that of our coronene cluster, 1.12 g/cm^3.

We have tested the effect of varying soot density on our soot model by studying a premixed laminar ethylene-oxygen-argon flame at atmospheric pressure with a carbon to oxygen ratio of 0.64 and a cold gas velocity of 7 cm/s as used in Ref. [31]. To do this, initially the ABF model [32] was employed using the method of moments, which we have implemented in the CHEMKIN package [33] and PREMIX [34]. We have modified the chemical mechanism by using a new rate for PAH oxidation [17]. The rate of soot surface growth is dependent on the surface area, which in turn depends upon the soot density. However, varying the density between 1.0 g/cm^3 and 2.0 g/cm^3 revealed no significant difference in the species concentrations. This result indicates that soot particle surface growth as specified by the ABF model is not strongly dependent on density. We also observed that as the mass density was doubled the soot mass fraction decreased by approximately 30%, whilst the peak particle number density increased by approximately 50%. The decrease in mass fraction is due to the reduced volume, and hence surface area, of denser particles which results in reduced rates of molecular surface growth and condensation of PAHs from the gas phase. Likewise, with less soot mass in the system, less coagulation is expected, which will increase the particle number density.

To understand how the density affects the particle size distribution we studied the same flame using a more complex soot model which used the KMC-ARS [13, 35] and PAH-PP [36**?**] models. With the simulated species profiles for $\rho = 1.8$ g/cm^3, found using the ABF model, PAH growth simulations were carried out using the KMC-ARS model. This model uses a kinetic Monte Carlo algorithm combined with a detailed reaction mechanism to simulate the growth of PAH molecules in flame conditions. One thousand 'PAH trajectories' were calculated describing the time evolution of the PAH molecules. Using these trajectories a multivariate PAH population balance model, named the PAH-PP model, was used to study the coagulation of PAHs, and hence the formation of soot particles. A given soot primary particle is composed of a list of known PAHs are hence the particle mass is known. Using the mass and the particle density the particle collision diameter can be calculated which in turn will affect the rate of further growth and aggregation. For full details of this soot model see Ref. [**?**].

In the simulations the particle mass density was varied from 1.0–1.8 g/cm^3 and size

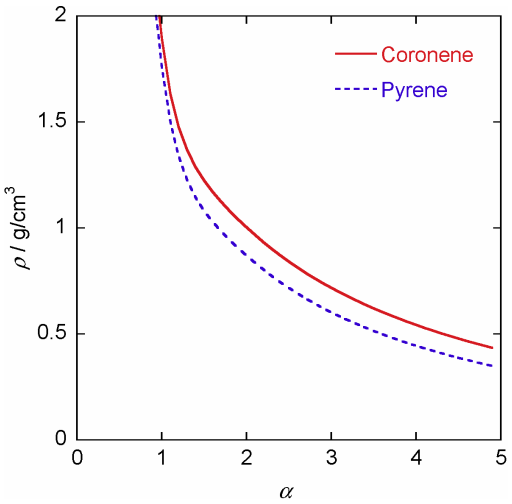

Figure 6: *Pure component cluster densities as a function of scaling factor.*

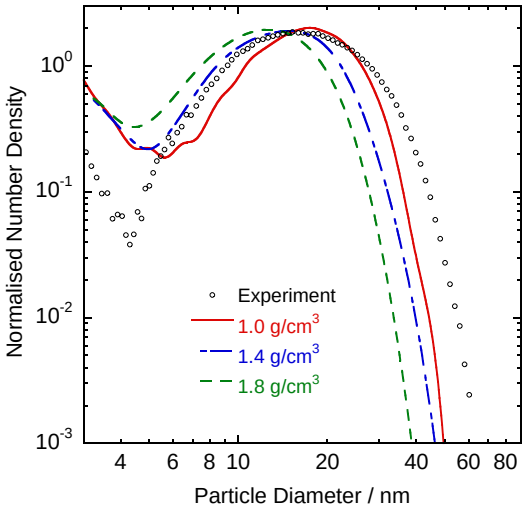

Figure 7: *Normalised number density distribution at 12 mm above the burner. The experimental data for this flame is from Ref. [31]*

distributions calculated over this range are shown in Fig. 7. To enable comparison with experimental results for this flame [31] only particles larger than 2.5 nm have been considered when constructing the particle size distribution. Typical bimodal distributions are found [9]: the first peak relating to small particles, and the second peak due to larger aggregates of smaller particles. At small particle diameters the simulation results overestimate the number density, however for larger particles peak number density matches well with experiment. As the particle density is increased a shift in the position of the aggregate peak of the distribution towards smaller particle diameters is observed. This trend indicates that particle density is an important parameter and should be considered alongside other parameters used in our soot models held constant during these simulations (*e.g.* the surface growth rate, the particle incepting species and the number of available active sites on the surface). It is interesting to note how the lower particle density simulations fit the experimental data more closely. In one of our previous publications [9] an attempt was

made to fit the experimental data by artificially increasing the fraction of active surface sites, *i.e.* in effect increasing the particle surface area which is equivalent to reducing the particle density. Whilst the soot model outputs are dependent upon many parameters, the current work suggests that a reduced soot particle density may be a better representation of the physical reality.

3 Conclusion

A simple Lennard-Jones plus point charges potential was used to generate potential energy surfaces for clusters of 50 coronene and 50 pyrene molecules, which have been explored using a basin-hopping algorithm. Energetically favourable configurations have been located and a TEM-style projection for a 50 molecule coronene cluster showed similarities with experimental TEM images of soot aggregates. The densities of these molecular clusters have been determined by defining cluster volume in terms of van der Waals radii and a critical scaling factor. The critical scaling factor was found to be 1.7 for both clusters. The resulting cluster densities were found to be 1.12 g/cm^3 for coronene and 0.98 g/cm^3 for pyrene, both being approximately 80% of the bulk crystalline values. The similarity of nascent soot particles with clusters of PAH molecules such as coronene and pyrene indicates that a density lower than the standard soot density of 1.8 g/cm^3 should be considered in our models. For modelling purposes we recommend the value of nascent soot density to be taken to be the value obtained for our coronene cluster of 1.12 g/cm^3. By varying soot particle density between 1.0 and 1.8 g/cm^3 in our soot models we have observed a noticeable shift in the particle size distribution towards smaller particle diameters, which highlights the importance of particle density as a parameter.

Acknowledgements

The authors would like to thank S. Mosbach and N. Morgan for useful discussions. T.S.T. gratefully acknowledges financial support from the EPSRC (under grant numbers EP/E01772X/1 and EP/G028672/1), Shell Research Ltd. and Churchill College, Cambridge.

References

[1] R. L. Vander Wal, A. Yezerets, N. W. Currier, D. H. Kim, and C. M. Wang. HRTEM Study of diesel soot collected from diesel particulate filters. *Carbon*, 45:70–77, 2007.

[2] T. Ishiguro, Y. Takatori, and K. Akihama. Microstructure of Diesel Soot Particles Probed by Electron Microscopy: First Observation of Inner Core and Outer Shell. *Combustion and Flame*, 108(1-2):231–234, 1997.

[3] J. Rodruez, J. Snchez-Marn, F. Torrens, and F. Ruette. Molecular aggregation of polycyclic aromatic hydrocarbons. a theoretical modelling of coronene aggregation. *Journal of Molecular Structure: THEOCHEM*, 254:429–441, 1992.

[4] C. A. Schuetz and M. Frenklach. Nucleation of soot: Molecular dynamics simulations of pyrene dimerization. *Proceedings of the Combustion Institute*, 29(2):2307–2314, 2002.

[5] R. Khanna, V. Sahajwalla, and R. H. Hurt. An atomistic technique for simulating non-covalent interactions in large ensembles of high-molecular-weight polyaromatics. *Carbon*, 43(1):67–77, 2005.

[6] M. Rapacioli, F. Calvo, F. Spiegelman, C. Joblin, and D. J. Wales. Stacked clusters of polycyclic aromatic hydrocarbon molecules. *Journal of Physical Chemistry A*, 109(11):2487–2497, 2005.

[7] D. Wong, R. Whitesides, C. A. Schuetz, and M. Frenklach. Molecular dynamics simulations of PAH dimerization. In H. Bockhorn, A. D'Anna, A. F. Sarofim, and H. Wang, editors, *Combustion Generated Fine Carbonaceous Particles*, pages 245–255. Karlsruhe University Press, 2007.

[8] M Balthasar and M Kraft. A stochastic approach to solve the particle size distribution function of soot particles in laminar premixed flames. *Combustion and Flame*, 133:289–298, 2003.

[9] J. Singh, R. I. A. Patterson, M. Kraft, and H. Wang. Numerical simulation and sensitivity analysis of detailed soot particle size distribution in laminar premixed ethylene flames. *Combustion and Flame*, 145:117–127, 2006.

[10] R. I. A. Patterson and M. Kraft. Models for the aggregate structure of soot particles. *Combustion and Flame*, 151:160–172, 2007.

[11] M. S. Celnik, R. I. A. Patterson, M. Kraft, and W. Wagner. Coupling a stochastic soot population balance to gas-phase chemistry using operator splitting. *Combustion and Flame*, 148(3):158–176, 2007.

[12] J. Singh, M. Balthasar, M. Kraft, and W. Wagner. Stochastic modelling of soot particle size and age distribution in laminar premixed flames. *Proceedings of the Combustion Institute*, 30:1457–1465, 2005.

[13] M. S. Celnik, A. Raj, R. H. West, R. I. A. Patterson, and M. Kraft. An aromatic site description of soot particles. *Combustion and Flame*, 155(1-2):161–180, 2008.

[14] N. Morgan, M. Kraft, M. Balthasar, D. Wong, M. Frenklach, and P. Mitchell. Numerical simulations of soot aggregation in premixed laminar flames. *Proceedings of the Combustion Institute*, 31(1):693–700, 2007.

[15] R. I. A. Patterson, J. Singh, M. Balthasar, M. Kraft, and J. Norris. The Linear Process Deferment Algorithm: A new technique for solving population balance equations. *SIAM Journal of Scientific Computing*, (28):303–320, 2006.

[16] R. I. A. Patterson, J. Singh, M. Balthasar, M. Kraft, and W. Wagner. Extending stochastic soot simulation to higher pressures. *Combustion and Flame*, 145(3):638–642, 2006.

[17] M. S. Celnik, M. Sander, A. Raj, R. H. West, and M. Kraft. Modelling soot formation in a premixed flame using an aromatic-site soot model and an improved oxidation rate. *Proceedings of the Combustion Institute*, 32(1):639–646, 2009.

[18] D. J. Wales and J. P. K. Doye. Global optimization by basin-hopping and the lowest energy structures of Lennard-Jones clusters containing up to 110 atoms. *The Journal of Physical Chemistry A*, 101(28):5111–5116, 1997.

[19] D. Chakrabarti and D. J. Wales. Simulations of rigid bodies in an angle-axis framework. *Physical Chemistry Chemical Physics*, 11(12):1970–1976, 2009.

[20] B. W. van de Waal. Calculated ground-state structures of 13-molecule clusters of carbon dioxide, methane, benzene, cyclohexane, and napthalene. *Journal of Chemical Physics*, 79(8):3948–3961, 1983.

[21] D. J. Wales and T. V. Bogdan. GMIN: A program for finding global minima and calculating thermodynamic properties from basinsampling. http://www-wales.ch.cam.ac.uk/GMIN.

[22] J. H. Miller, W. G. Mallard, and K. C. Smyth. Intermolecular potential calculations for polycyclic aromatic hydrocarbons. *Journal of Physical Chemistry*, 88(21):4963–4910, 1984.

[23] J. Appel, H. Bockhorn, and M. Wulkow. A detailed numerical study of the evolution of soot particle size distributions in laminar premixed flames. *Chemosphere*, 42(5-7):635–645, 2001.

[24] S. Mosbach, M. S. Celnik, A. Raj, M. Kraft, H. R. Zhang, S. Kubo, and K. Kim. Towards a detailed soot model for internal combustion engines. *Combustion and Flame*, 156(6):1156–1165, 2009.

[25] A. Bondi. van der Waals volumes and radii. *The Journal of Physical Chemistry*, 68(3):441–451, 1964.

[26] W. H. Press, S. A. Teukolsky, W. T. Vetterling, and B. P. Flannery. *Numerical Recipes in C++ The Art of Scientific Computing*. Cambridge University Press, Cambridge, 2nd edition, 2002.

[27] M. Alfe, B. Apicella, A. Tregrossi, and A. Ciajolo. Distribution of soot molecular weight/size along premixed flames as inferred by size exclusion chromatography. *Energy & Fuels*, 21(1):136–140, 2007.

[28] R. A. Dobbins, R. A. Fletcher, and H. C. Chang. The evolution of soot precursor particles in a diffusion flame. *Combustion and Flame*, 115(3):285–298, 1998.

[29] C. Park and J. P. Appleton. Shock-tube measurements of soot oxidation rates. *Combustion and Flame*, 20(3):369–379, 1973.

[30] M. Y. Choi, G. W. Mulholland, A. Hamins, and T. Kashiwagi. Comparisons of the soot volume fraction using gravimetric and light extinction techniques. *Combustion and Flame*, 102(1-2):161–169, 1995.

[31] B. Zhao, Z. Yang, Z. Li, M. V. Johnston, and H. Wang. Particle size distribution function of incipient soot in laminar premixed ethylene flames: effect of flame temperature. *Proceedings of the Combustion Institute*, 30(1):1441–1448, 2005.

[32] J. Appel, H. Bockhorn, and M. Frenklach. Kinetic modeling of soot formation with detailed chemistry and physics: Laminar premixed flames of C_2 hydrocarbons. *Combustion and Flame*, 121:122–136, 2000.

[33] R. J. Kee, F. M. Ropley, E. Meeks, and J. A. Miller. CHEMKIN-III: A FORTRAN chemical kinetics package for the analysis of gas-phase chemical and plasma kinetics. Technical Report UC-405 SAND96-8216, Sandia National Laboratories, Livermore, CA 94551-0969, USA, May 1996.

[34] R. J. Kee, K. Grcar, M. D. Smooke, and J. A. Miller. Premix: A fortran program for modelling steady laminar one-dimensional premixed flames. Technical Report UC-4 SAND85-8240, SANDIA National Laboratories, 1985.

[35] A. Raj, M. S. Celnik, R. Shirley, M. Sander, R. I. A. Patterson, R. H. West, and M. Kraft. A statistical approach to develop a detailed soot growth model using PAH characteristics. *Combustion and Flame*, 156(4):896–913, 2009.

[36] A. Raj, M. Sander, V. Janardhanan, and M. Kraft. A study on the coagulation of polycyclic aromatic hydrocarbon clusters to determine their collision efficiency. Technical Report 73, c4e Preprint-Series, Cambridge, 2009.